Quantum study of the Li+HF→LiF+H reaction

Alfredo Aguado, Miguel Paniagua, Manuel Lara, and Octavio Roncero

Citation: The Journal of Chemical Physics **107**, 10085 (1997); doi: 10.1063/1.474145
View online: http://dx.doi.org/10.1063/1.474145
View Table of Contents: http://scitation.aip.org/content/aip/journal/jcp/107/23?ver=pdfcov
Published by the AIP Publishing

Quantum study of the Li+HF→LiF+H reaction

Alfredo Aguado and Miguel Paniagua
Departamento de Química Física, Facultad de Ciencias C-XIV, Universidad Autónoma de Madrid, 28049 Madrid, Spain

Manuel Lara and Octavio Roncero
Instituto de Matemáticas y Física Fundamental, C.S.I.C., Serrano 123, 28006 Madrid, Spain

(Received 10 July 1997; accepted 9 September 1997)

In this work we present a new global fit for the potential energy surface of the LiFH system. This fit is an improvement of a recently published one [Aguado *et al.*, J. Chem. Phys. **106**, 1013 (1997)] for which more *ab initio* points have been calculated (from 644 to 2323). The reaction dynamics is studied using a time dependent treatment in reactant Jacobi coordinates in a body-fixed frame in which the internal coordinates are represented on a grid while Eulerian angles are described in a basis set. The centrifugal sudden approach is tested for total angular momentum $J=5$ and used to calculate the reaction cross section. The reaction cross section shows oscillations as a function of kinetic energy. This is a consequence of strong interference effects between reactant and product channels and is in agreement with the recent experimental data. © *1997 American Institute of Physics.* [S0021-9606(97)00547-3]

I. INTRODUCTION

The reactions between alkali or alkaliearth metal atoms and hydrogen halide molecules have attracted much attention from the first crossed beam experiment performed by Taylor and Datz.[1] In these systems the diatomic fragments have strong dipolar moments which allow both, the preparation of reagents in specific initial states and the determination of the final state of the products.[2,3] Moreover, it is possible to study the effect of the orientation of the reagents by introducing fields[4,5] or by producing aligned diatomic molecules using plane-polarized infrared light.[6]

In addition, these systems usually present a deep well in the entrance channel from which the system can be excited and the reaction dynamics studied at very precise energies. An increasing number of studies of these kind of photoinitiated reactions have been performed since the pioneering work of Soep,[7,8] Wittig[9] and their co-workers. This kind of experiments, in which the two reactants have a predetermined orientation within the complex, allows new transition state spectroscopy experiments,[10,11] which provides a direct information on the intermediates of the reaction and, therefore, on the reaction mechanism.

The Li+HF→LiF+H reaction, involving three different light atoms, is becoming a benchmark system to study elementary reactions due to its relative simplicity. The first crossed beam experiments on this system were performed by Lee and co-workers.[12] More recently the influence of the initial vibrational excitation of the reactants was studied by using an infrared laser to excite the HF molecule.[3,4,13,5] Moreover, by introducing an electric field it was possible to study the effect of the reagents relative orientation.[4,5]

From the theoretical point of view, the number of electrons is sufficiently low to perform high quality *ab initio* calculations,[14–17] and a wide variety of dynamical calculations on the reaction have been recently reported, using classical trajectories[18] and quantum treatments, either time-independent[19,20] or time-dependent.[21–23] In most of the dynamical calculations performed until today the Potential Energy Surface (PES) of Ref. 19 was used. This PES is based on a few *ab initio* points[15] but *ad hoc* modifications were introduced to reproduce experimental magnitudes. Such modifications caused some artificial features in the PES, such as an anomalous high barrier in the products channel. Very recently, a new PES was reported[22] based on about 600 MRDCI *ab initio* points[17] using the fitting procedure proposed by some of the authors.[24] However, the reactive cross section obtained with this last PES was low when compared with the experimental data.[12] This was due to the appareance of some artificial features in regions of the configuration space where no *ab initio* calculations were available.

In this work, we present a new global PES of the ground state of the LiFH system obtained by fitting a larger number of *ab initio* calculations (≈2300) which cover most of the relevant interaction region. Time-dependent calculations on the reaction dynamics of this system are also carried out for this new PES, using reactant Jacobi coordinates referred to a body-fixed frame. Within this treatment the internal coordinates are represented on discrete grids while the three Eulerian angles are described in a basis set. This procedure is very efficient because the PES is diagonal in this representation, which reduces the memory requirements. In addition, it is very well suited for massively parallel computing since the only coupling between different helicities is due to the Coriolis term. Thus the communication between processors is reduced by keeping each helicity component of the wave packet in a single processor. The centrifugal Sudden Approach[25] (CSA) is compared with exact calculations for $J=5$. Using this new PES within the CSA, the calculated reaction cross section is in excellent agreement with the available experimental data.[12,26] The role of initial reagent rotation is also examined.

II. QUANTUM TIME-DEPENDENT REACTIVE DYNAMICS

For the calculation of the total reaction probabilities, reactant Jacobi coordinates are used, in which the Hamiltonian takes the form

$$H=-\frac{\hbar^2}{2m}\left(\frac{2}{R}\frac{\partial}{\partial R}+\frac{\partial^2}{\partial R^2}\right)+\frac{\boldsymbol{l}^2}{2mR^2}-\frac{\hbar^2}{2\mu}\left(\frac{2}{r}\frac{\partial}{\partial r}+\frac{\partial^2}{\partial r^2}\right)+\frac{\mathbf{j}^2}{2\mu r^2}+V(r,R,\gamma)\ , \tag{1}$$

where $\mathbf{r}$ is the HF intramolecular distance, $\mathbf{R}$ goes from the HF center of mass to the Li atom, and γ is the angle between these two vectors. The angular momentum operators, $\mathbf{j}$ and $\boldsymbol{l}$ (and the corresponding reduced masses μ and m), are associated with $\mathbf{r}$ and $\mathbf{R}$, respectively, and $V(r,R,\gamma)$ is the interaction potential that will be discussed in detail in the next section.

It is convenient to use a body-fixed frame such that the z-axis lies along the $\mathbf{R}$ vector and all three atoms lie in the x-z plane. In this frame it can be distinguished between the internal coordinates, r, R and γ, and three Euler angles θ,ϕ and χ specifying the orientation of the body-fixed axis with respect to the space-fixed frame.[27] Thus, the angular momentum operators appearing in Eq. (1) are expressed as,[28]

$$\begin{aligned}
\mathbf{j}^2&=-\hbar^2\left\{\cot\,\gamma\frac{\partial}{\partial\gamma}+\frac{\partial^2}{\partial\gamma^2}+\frac{1}{\sin^2\,\gamma}\frac{\partial^2}{\partial\chi^2}\right\},\\
\mathbf{J}^2&=-\hbar^2\left\{\frac{\partial^2}{\partial\theta^2}+\cot\,\theta\frac{\partial}{\partial\theta}+\frac{1}{\sin^2\,\theta}\left(\frac{\partial^2}{\partial\phi^2}+\frac{\partial^2}{\partial\chi^2}-2\cos\,\theta\frac{\partial^2}{\partial\chi\partial\phi}\right)\right\},\\
\mathbf{J}\cdot\mathbf{j}&=-\hbar^2\left\{(1-\cot\,\gamma\,\cot\,\theta\,\cos\,\chi)\frac{\partial^2}{\partial\chi^2}-\cot\,\theta\,\sin\,\chi\frac{\partial^2}{\partial\chi\partial\gamma}+\cos\,\chi\frac{\partial^2}{\partial\theta\partial\gamma}\right.\\
&\quad+\frac{\cot\,\gamma\,\cos\,\chi}{\sin\,\theta}\frac{\partial^2}{\partial\phi\partial\chi}+\frac{\sin\,\chi}{\sin\,\theta}\frac{\partial^2}{\partial\phi\partial\gamma}\\
&\quad\left.-\cot\,\gamma\,\sin\,\chi\frac{\partial^2}{\partial\theta\partial\chi}\right\},
\end{aligned} \tag{2}$$

with $\boldsymbol{l}^2=\mathbf{J}^2+\mathbf{j}^2-2\mathbf{J}\cdot\mathbf{j}$.

The total wavepacket is expanded as

$$\Psi^{JMp}(\mathbf{R},\mathbf{r},t)=\sum_{\Omega\geqslant 0}^{J}W^{Jp}_{M\Omega}(\phi,\theta,\chi)\frac{\Phi^{JMp}_{\Omega}(r,R,\gamma,t)}{rR}, \tag{3}$$

where the $W^{Jp}_{M\Omega}$ functions are linear combinations of Wigner rotation matrices[27] such that the parity under inversion of all coordinates, p, is well defined,

$$W^{Jp}_{M\Omega}(\phi,\theta,\chi)=\sqrt{\frac{2J+1}{16\pi^2(1+\delta_{\Omega,0}}}\times[D^{J*}_{M,\Omega}(\phi,\theta,\chi)+p(-1)^J D^{J*}_{M,-\Omega}(\phi,\theta,\chi)], \tag{4}$$

M and Ω being the quantum numbers for the projections of the total angular momentum, $\boldsymbol{J}$, on the space-fixed and body-fixed z-axis, respectively. Insertion of Eq. (3) into the time-dependent Schrödinger equation using the Hamiltonian of Eq. (1), yields a set of first order-differential equations for the $\Phi^{JMp}_{\Omega}(r,R,\gamma,t)$ coefficients,

$$\begin{aligned}
i\hbar\frac{\partial\Phi^{JMp}_{\Omega}(r,R,\gamma,t)}{\partial t}&=\left[-\frac{\hbar^2}{2m}\frac{\partial^2}{\partial R^2}-\frac{\hbar^2}{2\mu}\frac{\partial^2}{\partial r^2}+\frac{\mathbf{j}^2}{2\mu r^2}+V(r,R,\gamma)\right]\\
&\quad\times\Phi^{JMp}_{\Omega}(r,R,\gamma,t)\\
&\quad\times+\sum_{\Omega'}\left\langle W^{Jp}_{M\Omega}\left|\frac{\boldsymbol{l}^2}{2mR^2}\right|W^{Jp}_{M\Omega'}\right\rangle\Phi^{JMp}_{\Omega'}(r,R,\gamma,t).
\end{aligned} \tag{5}$$

The integration of these equations is performed using the Chebyshev method[29] and the $\Phi^{JMp}_{\Omega}(r,R,\gamma,t)$ coefficients are represented on finite grids for the internal coordinates r, R, γ. A set of equidistant points, r_n,R_m, is chosen for the two-dimensional radial grid, and the radial kinetic term is solved using the Fast Fourier Transform method.[30] In the calculations presented below the typical radial grid is composed by 176×384 points in the interval $0.25\leqslant r_n\leqslant 8.25$, $0.5\leqslant R_m\leqslant 17.5$ Å. In order to avoid artificial reflections, due to the use of a finite grid, the wavepacket is absorbed after each time step: The wavepacket to be used in the next time step is replaced by $\Psi(t)f_1(r)f_2(R)$, where $f_i(x)=\exp[-\beta_i(x-x^{abs})^2]$ if $x>x^{abs}$ and $f_i(x)=1$ otherwise, with $r^{abs}=4$ and $R^{abs}=14.5$ Å. (The exponential parameters β_i are chosen to minimize the effect on the wavepacket.)

For γ, we use a set of 25–30 Gauss–Legendre quadrature points, γ_k, with weights w_k. The actual $\Phi^{JMp}_{\Omega}(r_n,R_m,\gamma_k,t)$ already includes the factor $\sqrt{w_k}$ to simplify the numerical integration over the γ variable. The action of the angular momentum operators on the wavepacket, diagonal in the radial grid representation, is performed in a single operation[31–36] as a simple multiplication of a matrix by a vector since

$$\hat{\mathscr{O}}_{\Omega',\Omega}\sum_k\Phi^{JMp}_{\Omega}(r_n,R_m,\gamma_k,t)=\sum_{k,k'}A^{\Omega',\Omega}_{k',k}(\hat{\mathscr{O}})\Phi^{JMp}_{\Omega}(r_n,R_m,\gamma_k,t), \tag{6}$$

where $\hat{\mathscr{O}}_{\Omega',\Omega}\equiv\langle W^{Jp}_{M\Omega'}|\mathbf{j}^2|W^{Jp}_{M\Omega}\rangle$ or $\langle W^{Jp}_{M\Omega'}|\boldsymbol{l}^2|W^{Jp}_{M\Omega}\rangle$ and the corresponding matrices are

$$A^{\Omega',\Omega}_{k',k}(\mathbf{j}^2)=\delta_{\Omega',\Omega}\hbar^2\sum_{j}^{j^{max}}\sqrt{w_{k'}}Y_{j\Omega}(\gamma_{k'},0)\times j(j+1)\sqrt{w_k}Y_{j\Omega}(\gamma_k,0),$$

$$A^{\Omega',\Omega}_{k',k}(\boldsymbol{l}^2)=\hbar^2\sum_{j}^{j^{max}}\sqrt{w_{k'}}Y_{j\Omega'}(\gamma_{k'},0)\sqrt{w_k}Y_{j\Omega}(\gamma_k,0)\times\{\delta_{\Omega,\Omega'}[J(J+1)+j(j+1)-2\Omega^2]-\delta_{\Omega,\Omega'\pm1}\sqrt{1+\delta_{\Omega,0}+\delta_{\Omega',0}}\sqrt{J(J+1)-\Omega\Omega'}\times\sqrt{j(j+1)-\Omega\Omega'}\},\tag{7}$$

where $j^{max}\leqslant k^{max}-1$, k^{max} being the number of Gauss–Legendre points used to describe the γ variable.

It is convenient to use this mixed representation, a Finite Basis Representation (FBR) for the Euler angles and a Discrete Variable Representation (DVR) for r,R and γ, because the interaction potential is diagonal in the representation of all the internal coordinates, which reduces considerably the storage requirements, as has being recently reported.[36] In addition, it turns out that the only coupling between adjacent Ω components of the total wavepacket is due to the non-diagonal terms of $\boldsymbol{l}^2$. This calculation is very well suited for massively parallel computing: each processor is assigned a value of Ω, and the exchange of information between processors is only due to the non-diagonal terms of $\boldsymbol{l}^2$.[36]

The wavepacket at $t=0$ is defined by the simple product,

$$\Psi^{JMp}(\mathbf{R},\mathbf{r})=W^{Jp}_{M\Omega_0}Y_{j_0,\Omega_0}(\gamma,0)\frac{\phi_{v_0,j_0}(r)}{r}\frac{G(R)}{R},\tag{8}$$

where $\phi_{v_0,j_0}(r)$ is an eigenstate of HF, i.e.,

$$\left\{-\frac{\hbar^2}{2\mu}\frac{\partial^2}{\partial r^2}+\frac{\hbar^2 j(j+1)}{2\mu r^2}+V(r,R\to\infty,\gamma)-E_{v,j}\right\}\phi_{v,j}=0,\tag{9}$$

and $G(R)$ is a complex Gaussian function of the form

$$G(R)=\left(\frac{2}{\pi\Gamma^2}\right)^{1/4}\exp\left[-\frac{(R-R_0)^2}{\Gamma^2}-i\mathscr{K}_0R\right].\tag{10}$$

This function is centered at an initial value $R_0=13$ Å , in the asymptotic region, with an approximate mean kinetic energy of $\hbar^2\mathscr{K}_0^2/2m\approx0.2$ eV. Γ, related to the width of the energy distribution, is chosen in such a way that the energy dispersion of the wave packet is one third of the initial mean kinetic energy.

The energy-resolved total reaction probability is calculated from the total flux of the energy projection of the wave packet through a surface in the products region at $r^*=3$ Å as[37–40]

$$P^{Jp}_{v_0,j_0,\Omega_0}(E)=\sum_{v',j',\Omega'}|S^{Jp}_{v_0,j_0,\Omega_0\to v',j',\Omega'}(E)|^2=\frac{\hbar^2K_0(E)}{4\pi^2\mu m}\sum_{\Omega}\int dR\ \sin\gamma d\gamma\times\mathrm{Im}\left[\Psi^{+}_{\Omega}{}^{*}(r^*,R,\gamma,E)\frac{\partial\Psi^{+}_{\Omega}(r,R,\gamma,E)}{\partial r}\bigg|_{r^*}\right],\tag{11}$$

where v',j',Ω' are the quantum numbers specifying the final state of the LiF products, $K_0(E)=\sqrt{2\mu(E-E_{v_0,j_0})}/\hbar$. The time-independent wavefunctions Ψ^{+}_{Ω} are defined as

$$\Psi^{+}_{\Omega}(r,R,\gamma,E)=\frac{1}{a_0(E)}\int_{-\infty}^{\infty}dt e^{iEt/\hbar}\Phi^{JMp}_{\Omega}(r,R,\gamma,t),\tag{12}$$

with

$$a_0(E)=\frac{1}{2\pi}\int dR e^{iRK_0(E)}G(R).\tag{13}$$

By defining the helicity averaged reaction probability for a given J as[41]

$$P^{J}_{v_0,j_0}(E)=\frac{1}{2j_0+1}\sum_{p=\pm1}\sum_{\Omega_0=\Omega_0^p}^{j_0}P^{Jp}_{v_0,j_0,\Omega_0}(E),\tag{14}$$

where $\Omega_0^p=0$ or 1 for $p=(-1)^J$ and $p=(-1)^{J+1}$, respectively, the total reaction cross section becomes

$$\sigma_{v_0,j_0}(E)=\frac{\pi}{K_0^2}\sum_{J=0}^{\infty}(2J+1)P^{J}_{v_0,j_0}(E).\tag{15}$$

The evaluation of the total reaction cross-section requires to go up to high J values (of the order of 60 for this system) in the wavepacket calculations. To avoid the difficulty of these very expensive calculations some approximations are introduced. (Such approximations will be checked for $J=5$ below in section IV.) In the ''Centrifugal Sudden Approach''(CSA)[28,42,43] the projection of $\mathbf{j}$ on the z body-fixed axis, Ω, is conserved, since, the only coupling between different helicity states in Eq. (5), arises from the $\mathbf{J}\cdot\mathbf{j}$ term on the Hamiltonian. Such an approximation involves $\mathbf{J}\cdot\mathbf{j}\approx-\hbar^2(\partial^2/\partial\chi^2)$, in Eq. (2). Therefore, in this approach the sum over $\Omega'\neq\Omega$ disappears in Eqs. (5) and (11), and the calculation at any J value is computationally equivalent to that of $J=0$. This approximation strongly depends on the choice of the body-fixed axis. For Li+HF in reactant Jacobi coordinates, however, the body-fixed z-axis approximately coincides with the principal inertia axis, which suggests that the Coriolis coupling is small.

A further approximation is the so-called ''J-shifting''[25,44,45] based on the transition state theory, in which it is considered that the centrifugal barrier $\hbar^2[J(J+1)-2\Omega^2]/2mR^2$ appearing in the CSA only produces a shift on the reaction probabilities for different J values, i.e.,

$$P^{J}_{v_0j_0\Omega_0}(E)\approx P^{J=0}_{v_0j_0}(E-B[J(J+1)-2\Omega^2]),\tag{16}$$

where $B=\hbar^2/2mR^{\ddagger2}$, $R^{\ddagger}$ being the R value at the transition state.

III. POTENTIAL ENERGY SURFACE

The present wavepacket calculations employs an improved potential energy surface with respect to our previous one[22] (thereafter referred as PES1). Our earlier PES1 was constructed using the set of 570 *ab initio* values of Ref. 17, and an additional set of 74 computed energies for longer LiF distances at several angles of approach keeping HF at its equilibrium distance. However, the basic grid of geometries did not include points for interatomic distances longer than 4 Å for the reactants channel and 2.5 Å for the products channel. The only information for longer distances was given by the two-body potentials and two points included to obtain the reaction endoergicity. In addition, the basic grid of *ab initio* values was constructed by varying the HF distance by (in Å)

$$R_{HF}=0.9+0.265\ i \quad (i=-1,0,1,2,3,4,5).$$

Here, the spacing is larger than the distance between the two classical turning points of free HF (≈0.2 Å), and, therefore, there is no detailed information around the equilibrium distance of HF in the entrance channel. As a consequence, the HF distance at the well in the entrance channel (the absolute minimum in the PES) was found to be 0.929 Å, only 0.08 Å larger than the equilibrium distance of free HF simply as a consequence of the interpolation produced in the fit of PES1. Moreover, this lack of *ab initio* information is responsible for the presence, in PES1, of a repulsive wall in the reactants channel at longer HF distances than would be expected. This causes a considerably reduced ''cone of acceptance'' in PES1 with important consequences on reactivity.

Due to the above arguments, we have extended our *ab initio* calculations over a wider domain of the configuration space using the same multi-reference single and double excitations configuration interaction technique (MRDCI).[46] The basis set and the reference configurations were the same as in our previous calculations.[17] Accordingly, we enlarge the basic grid of geometries by including new points corresponding to longer interatomic distances for all the θ angles of approach (θ being the $\widehat{\mathrm{LiFH}}$ corresponding angle in internal coordinates). Moreover, complete grids for new θ angles are computed, in particular for 30° and 45°. We include also new points at geometries close to the HF and LiF equilibrium distances in order to get more information about the reactants and products channels. The new set of *ab initio* values contains 2323 points, i.e., about four times our previous data set. We stress that this new set of *ab initio* points covers more faithfully not only the asymptotic regions but also regions where a lack of information was noticeable.

Here, the LiFH adiabatic potential corresponding to the $^2A'$ ground state is fitted using the same global procedure as in Ref. 24. The two-body potentials have not been modified with respect to the previous ones (see Table I in Ref. 22). The three-body term of the potential is expressed as a polynomial of order 9 in the same Rydberg type variables as before, but using all the 2323 calculated MRDCI energies for the new fit. This new PES has a root-mean-square error of 0.03 eV and a maximum deviation of 0.16 eV (corresponding to one data point with energy higher than 5 eV) and will be referred to as PES2 in what follows. The parameters of the fit (192 linear parameters and 3 nonlinear parameters) are available from the authors upon request.[47] In Table I we give a summary of the stationary points corresponding to the present fit (PES2) including the zero-point energies for all of them. The transition state has been lowered about 0.03 eV with respect to our previous PES1[22] but including the zero-point energy this lowering is reduced to 0.006 eV, i.e., a negligible quantity. The diatomic reactants and products have been not modified with respect to PES1. Nevertheless, the complex has modified its position in the reactants channel and has now a longer HF distance (0.939 Å) and a shorter LiF distance (1.880 Å) than in PES1. Moreover, the well in the products channel (named the second well in Table I) has changed significantly.

TABLE I. Stationary points on the LiHF PES.

	Reactants	Complex	Transition state	Second well	Products
R_{LiF} (Å)	∞	1.880	1.692	1.601	1.587
R_{HF} (Å)	0.921	0.939	1.301	2.533	∞
θ_{LiFH}	—	107.4	71.4	85.7	—
E (eV)	0.	−0.279	0.233	0.019	0.082
$E+E_0$ (eV)	0.254	−0.007	0.322[a]	0.081	0.137

[a]Obtained in a calculation in reactant Jacobi coordinates with the r frozen, $r=1.301$ Å, since at the saddle point the reaction path nearly coincides with the HF internuclear distance.[22]

The contour maps of the *ab initio* PES2 corresponding to several angles of approach (θ) are generated. The maps are very similar to those obtained for the previous PES1 (see figure 1 in Ref. 22). In order to compare better PES1 with PES2, different potential energy contour maps are reported here, Figs. 1 to 3, for three constant HF distances. These three selected HF distances correspond approximately to the two classical turning points for HF in its ground vibrational state at about 0.25 eV (Figs. 1 and 3) and to the equilibrium HF distance (Fig. 2). As can be appreciated in Fig. 1, the repulsive wall encountered by the Li atom in the PES1 as it approaches the HF molecule is about 0.15 eV higher than the reactants. A very different situation occurs in PES2, where the energy goes down as the Li atom approaches the HF molecule. In Fig. 2, for the HF distance fixed at its equilibrium position (0.921 Å), the two PES's are very similar except for small angles of approach where the new PES2 presents a small well corresponding to the approach of the Li atom to the HF molecule from the H end. Finally, in Fig. 3, for the HF distance fixed at 1.027 Å, the PES1 shows oscillations at intermediate distances that are not present in our new PES2. Here, the PES2 shows the well for small angles of approach as in Fig. 2.

IV. RESULTS AND DISCUSSIONS

A. Dynamics for zero total angular momentum

The reaction probability for Li+HF ($v_0=0,j_0=0$,J=0), in Fig. 4, shows sharp resonance structures superimposed to

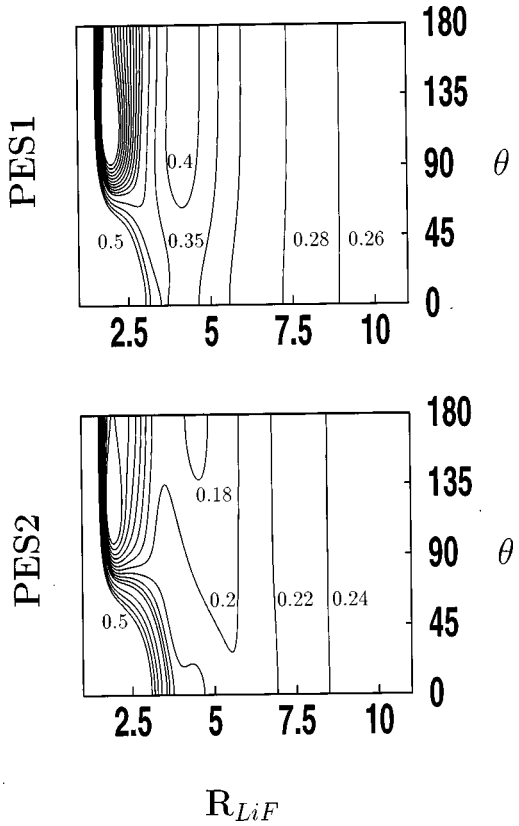

FIG. 1. Potential energy contour maps as a function of the LiF distance (in Å) and the LiFH angle θ, with the HF distance fixed at 0.837 Å. The curves are contours of the interaction potential corresponding to the following: from 0.1 to 0.3 with increments of 0.02, 0.35, 0.40, 0.45 and 0.50 eV. The top panel corresponds to our previous PES1,[22] the bottom panel corresponds to the present PES2.

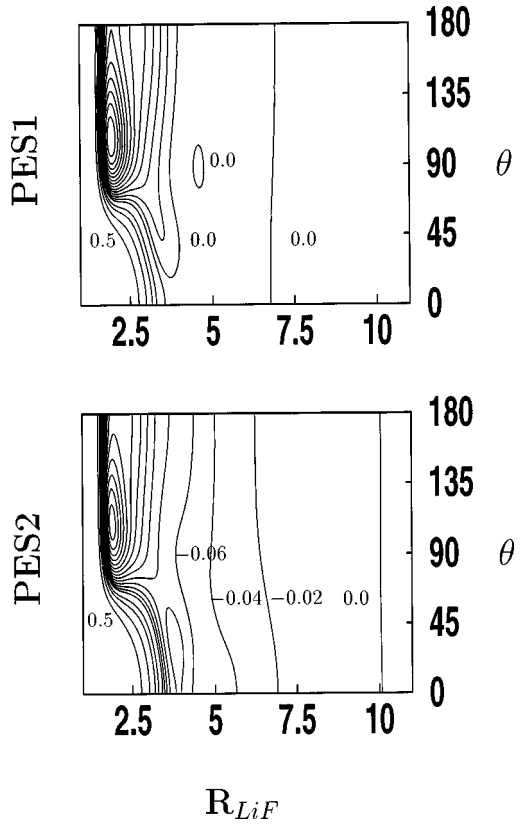

FIG. 2. The same as Fig. 1 but for the HF distance fixed at 0.921 Å. The countours correspond to the following: from −0.26 to 0.0 with increments of 0.02, 0.05, 0.1, 0.2 and 0.4 eV.

a slow oscillating envelope. The oscillations of the background envelope are due to quantum interference between the reactant and product channels.[19] Its associated frequency is ≈70 meV, and it seems nearly constant in all the energy range studied. The energy mismatch between the reactant and the product diatomic molecules, in their ground states, is of 116 meV.[22] The reason why these two quantities do not agree is probably because the LiF fragments are produced in excited rotational states. Previous quantum studies on this reaction[19,21] but using a different PES[19] (hereafter referred to as PES3) also found an analogous pattern. However, the background oscillations are only apparent in the reaction probability for particular final states of LiF, and are washed out when summing over all final states of the products,[19,21,23] because the different final states are produced with different interference pattern. Then, the interference pattern is so important for the total reaction probability in PES2 probably because only a few final states of LiF are formed. In a forthcoming work, an analysis of the final state of the products will be presented and this fact will be discussed in more detail.

For this reaction the energy of the barrier at the saddle point is lower than that of the ground level of the HF reactant, and, in principle, there is no translational energy threshold. However, if the zero-point energy of the transition state is taken into account, a threshold appears at 68 meV of translational energy, which explains the low, although raising, reaction probability at low energies. In this energy region, the reaction is dominated by a dense manifold of resonances, attributed to the presence of deep wells in the reactant and product valleys. In Fig. 5 a detailed plot for low translational energy is shown. The mean separation between adjacent resonances is of the order of ≈1–3 meV, and the lifetime of the three more intense resonances is of the order of 0.5 ps, being usually larger for the rest of them. We want to stress that the reactivity at some of the resonances increases significantly and its direct study by a photon-induced experiment can help in understanding the nature of the transition states and the reaction mechanisms. The LiHF complex has an important dipolar moment. Therefore, in principle, it is possible to design an experimental set up in which the complex is formed in the reagent well and then promoted to this resonant-mediated regime by infrared photon excitation.

The energy grid resolution used is of ≈ 0.25 meV and the propagation was performed until 9 ps. The S^2 matrix elements for the inelastic process $Li+HF(v_0,j_0)\rightarrow Li+ HF(v,j)$ were also calculated using the method of Balint-Kurti *et al.*[48,49] Roughly, the calculation of the individual S^2 matrix elements involves the ratio between the probability in the exit channel at a long time and the probability in the entrance channel at the initial time, both evaluated at a specific energy. The energy projection of the wavepacket at a long time

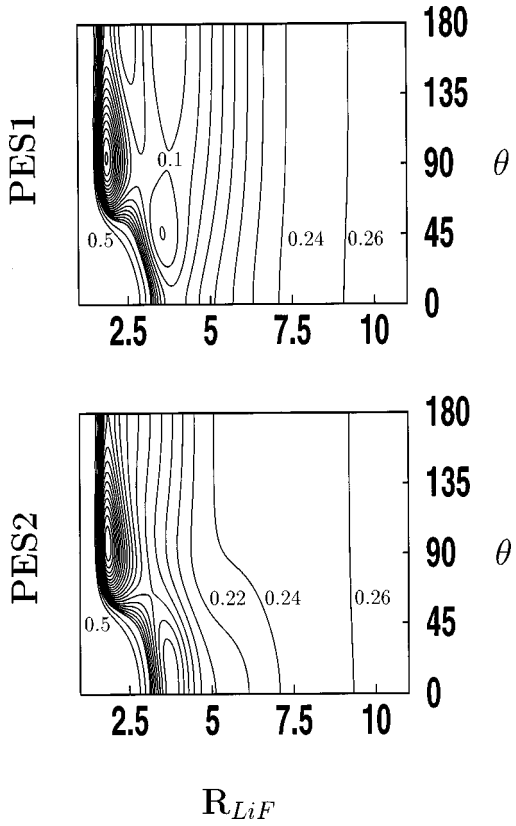

FIG. 3. The same as Fig. 1 but for the HF distance fixed at 1.027 Å. The countours correspond to the following: from −0.2 to 0.26 with increments of 0.02, 0.35 and 0.5 eV.

suffers some inaccuracy due to the numerical propagation, and this error increases with the number of integration steps. Since each S^2 matrix element is evaluated independently, the sum of all of them on a column, which should be 1, is used to establish the accuracy of the calculation and to determine whether or not the propagation is long enough. The sum of the S^2 matrix elements, in Fig. 4, only shows local

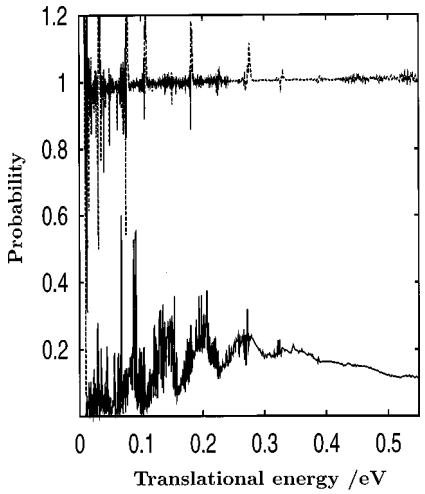

FIG. 4. The reaction probability for Li+HF(v_0=0, j_0=0, J=0) versus translational energy. As an accuracy check, the sum of all S^2 matrix elements, including the inelastic ones, is also plotted, in dashed lines.

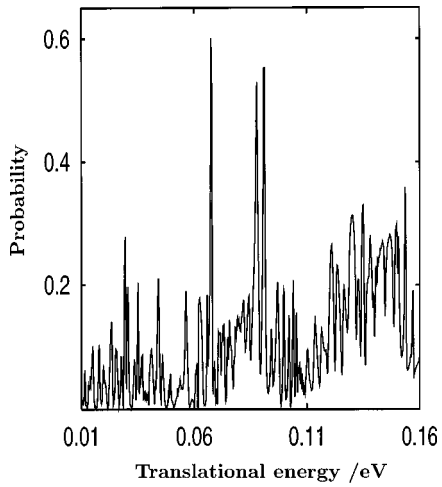

FIG. 5. Details of Fig. 4 in the region dominated by resonances.

deviations from the exact unity value in the vicinity of some resonances and at very low kinetic energies. The reaction probability is well converged after 3 ps while the S^2 matrix elements corresponding to the inelastic scattering takes a longer time just because the absorption distance for this channel, at which the S^2 is calculated, is placed at longer distances since the HF–Li interaction is of a longer range than the LiF–H one. The local inaccuracy of the sum of the S^2 matrix elements is mainly attributed to the inelastic channels since they imply longer time propagation and, therefore, larger numerical errors. We conclude that the resonant structure in the reaction probability is essentially correct and the inaccuracy at some energies can be quantified by the sum of all the S^2 matrix elements.

The transition state for this system has a bent geometry with a narrow passage between the reactant and product valleys, which suggests that the reaction strongly depends on the rotational state of the reactants. The effect of the reagent rotation has been the subject of great interest,[50–52] leading to simple models as the ''rotational'' sliding mass one,[51] but in general it is not always possible to predict the effect of the reagent rotation on the reaction cross sections. The reaction probabilities for inital rotational excitation j_0=0 and 1, in Fig. 6, are very similar. The resonances are more clearly exhibited for j_0=0 than for j_0=1, but they both show the same resonant structure. The background oscillations are also similar for these two cases, but for j_0=1 the probability is slightly shifted towards higher energy. The situation for j_0=2 is quite different. The background oscillations are missing and the reaction probability is significantly reduced. Such an effect can not be attributed to the higher initial energy for j_0=2. For j_0=3 the reaction probability is between those of j_0=1 and j_0=2, as has also been found in classical trajectories.[53] We conclude that on average the reaction probability decreases with increasing j_0, since the reaction takes place at quite a precise orientation between the HF and Li reactants which is disrupted by the increase of rotational excitation.

For the PES3, the reaction probability shows a distinct

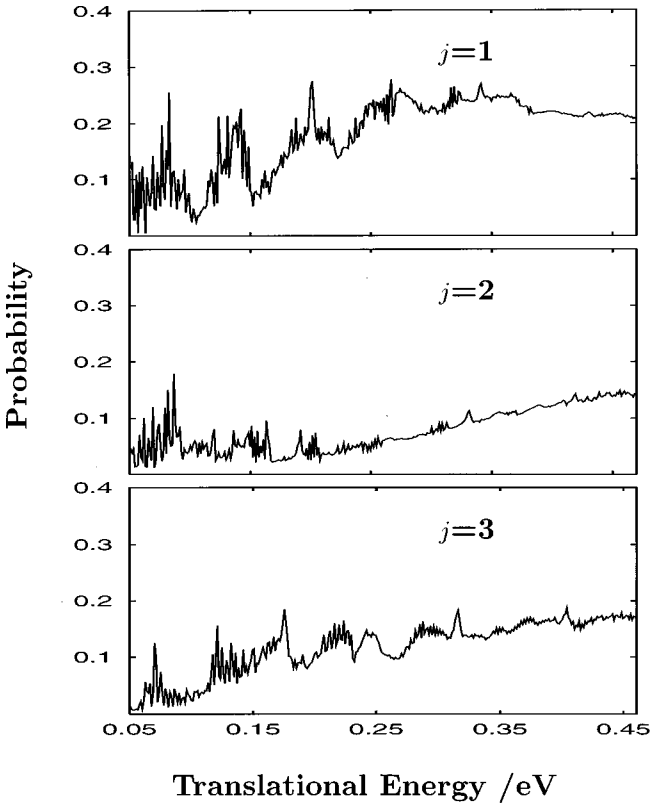

FIG. 6. Reaction probabilities for Li+HF($v_0=0$, j_0, $J=0$) versus translational energy for the different rotational excitation of HF.

behavior for even and odd j_0 values and no substantial reduction of the reaction probability as a function of j_0.[19,21,23] In the PES3 the interaction between the reactants ends at shorter distances than in PES2, and its anisotropy is also lower. Therefore, the rotational channels are more strongly mixed in PES2 than in PES3. Assuming that in PES3 the odd terms in a Legendre polynomial expansion are small in the entrance channel, even and odd j values are approximately decoupled which would explain the reaction probability difference between $j_0=0$, 2 and $j_0=1$, 3.

As it was stressed in the previous section, PES2 implies an improvement with respect to PES1 because of the larger number of *ab initio* points. At a first glance the two surfaces look very similar and the differences arising in the product region are not considered to be responsible for the large discrepancies in reactivity. In the reactants region the most important difference is that PES1 shows oscillations at intermediate distances. These oscillations produced by the fit[22] are of the order of $\approx$ 6 meV for the equilibrium distance of free HF, r_e, but the barrier increases with decreasing r, as has been discussed in the previous section. The inclusion of new *ab initio* points to produce the PES2, however, eliminates such oscillations. Since the ''cone of acceptance'' is larger in PES2 than in PES1, the reactivity in PES1 is much lower (see Fig. 7) than in PES2 (in Figs. 4 and 6). Reduced dimensionality calculations were performed for PES1 and PES2, within the Infinite Order Sudden Approximation (IOSA), i.e., solving a two-dimensional problem in r and R for each γ value. The IOSA averaged reaction probabilities

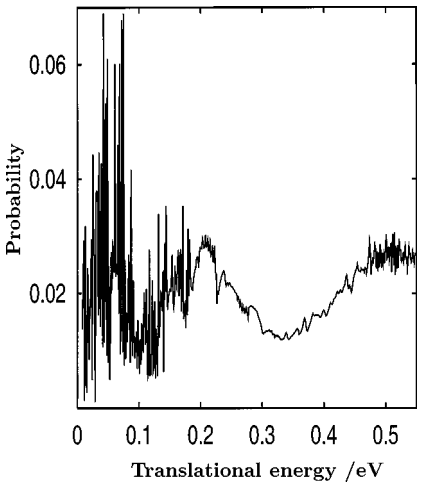

FIG. 7. Same as Fig. 4, but using PES1 of Ref. 22.

obtained for PES1 and PES2 were nearly identical, with a small energy shift due to the different height of the saddle point, of the order of $\approx$18 meV. Therefore, the reduction of the cone of acceptance on the HF internuclear distance has not a direct effect on reactivity. It has an indirect effect when the rotational motion is included: The high barrier appearing at short r distances produces a very high excitation on the rotation of the HF thus preventing the reactants to take the required reaction orientation.

B. Exact and approximated calculations for $J>0$

The z-axis of the body-fixed frame lies along the **R** vector which joins the Li atom to the HF center of mass. Since H is rather light, as compared with the other two atoms, it can be assumed that the z-axis chosen nearly coincides with the principal axis of inertia of the system. Therefore the Coriolis term, which is the only one that couples different Ω channels, should be rather small. Several exact calculations for $v_0=0$, $j_0=0$ and $J>0$ have been performed and in Fig. 8 the population of the Ω components of the wavepacket

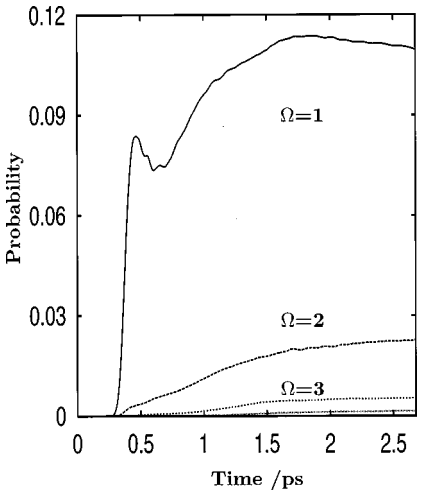

FIG. 8. The population of the Ω components of the exact wavepacket versus time for the Li+HF($v_0=0$, j_0) collision and $J=5$.

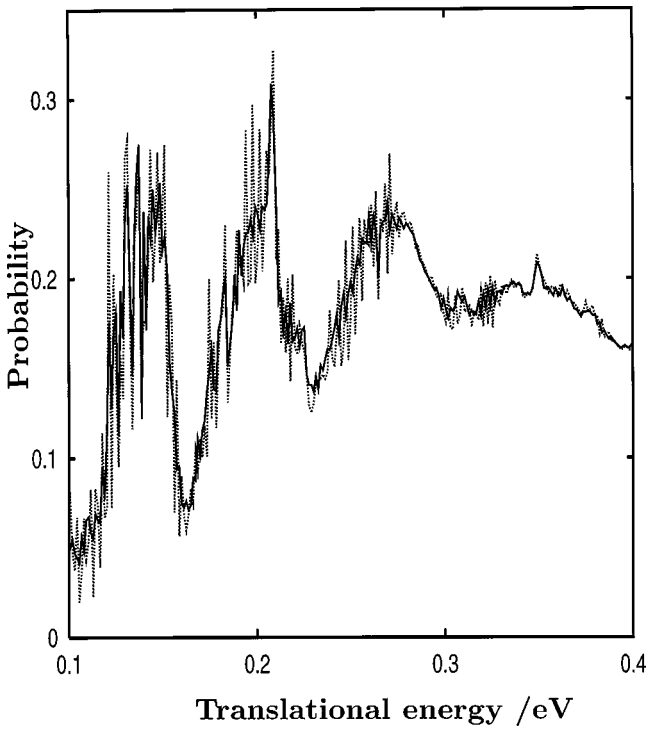

FIG. 9. Reaction probabilities for Li+HF($v_0=0$, j_0, $J=5$): the full lines correspond to the exact treatment while the dashed lines are the CSA results.

versus time is shown for the case of $J=5$. There is a significant mixing between the different Ω values so that the population on the initial $\Omega_0=0$ gets down to $\approx 86\%$. As expected, there is a decreasing importance on the populations as Ω increases, becoming nearly negligible for $\Omega=5$, $\approx 0.02\%$. Such mixing increases proportionally to J^2, since the coupling is proportional to J. As the mean Ω value increases, the effective rotational barrier gets lower and the threshold of the reaction can therefore vary.

In Fig. 9 the reaction probability obtained using the exact treatment is compared with the Centrifugal Sudden Approach, in which only $\Omega=0$ is included. The two results were obtained after propagating the wavepacket up to the same time in the two treatments, ≈ 2.5 ps, in order to avoid discrepancies. The exact and CSA reaction probabilities shows the same background envelope, and it does not seem that the Ω mixing produces any significant shift. In addition, the resonances appear to be located at the same energies, up to the resolution imposed by the energy grid used to evaluate the reaction probabilities. However, the CSA seems to overestimate the intensity of the resonances with respect to the exact treatment. Since the exact calculation includes $\Omega=0,1,...,5$, for $p=(-1)^J$, there are 6 rotational sublevels for each one appearing in the CSA where only $\Omega=0$ is considered. That rotational manifold of levels are close and are coupled through the Coriolis term, so that each of the resulting resonances have a contribution on $\Omega=0$. Since the main component of the wavepacket is $\Omega=0$, in the exact treatment there will be about 6 resonances each of them with a lower intensity in the reaction probability, approximately proportional to the weight of the $\Omega=0$ component of the reso-

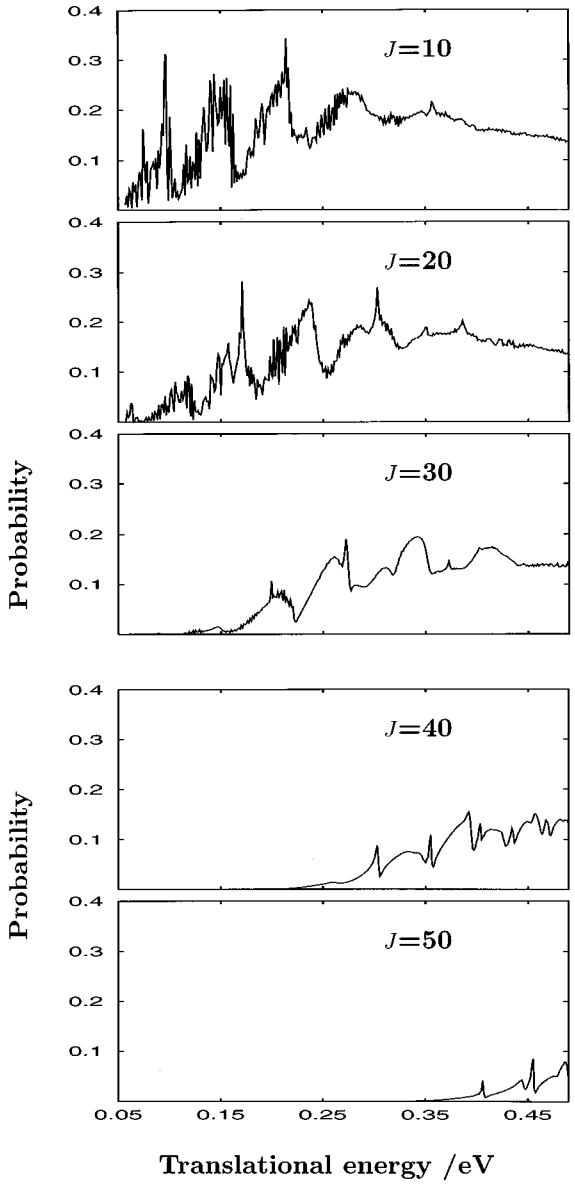

FIG. 10. Reaction probabilities for Li+HF($v_0=0$, j_0, J) for several values of the total angular momentum using the CS approach.

nance. In addition, those resonances are not resolved because the splitting is small as compared with the energy grid used. Aside from this problem, the CSA results are in excellent agreement with the exact ones, and extrapolating this result for higher J's it can be concluded that the CSA will yield essentially good estimates of the reaction cross section.

The exact calculation of higher J becomes computationally very expensive and will be the subject of future work. Instead, to evaluate the total reaction cross-section we shall use the CSA. In Fig. 10 we report the reaction probabilities obtained for several values of J using the CSA. As expected, the probability shifts towards higher energies as J increases. For low J's ($J<20$), this shift does not strongly affect the energy dependence of the reaction probability. The resonances become broader but the background envelope seems to correspond to a shift in agreement with the J-shifting ap-

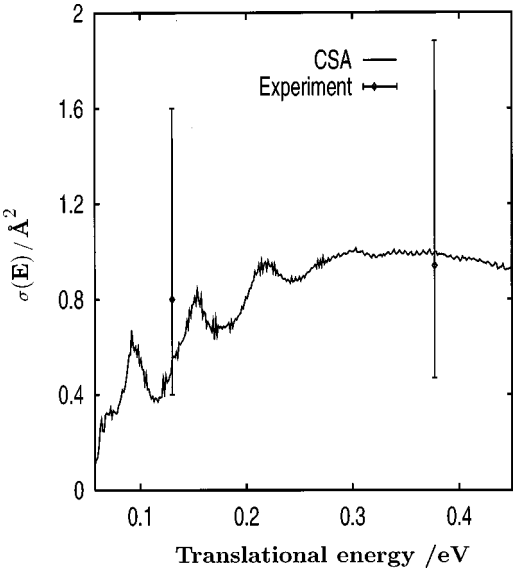

FIG. 11. The total reaction cross section for the Li+HF($v_0=0,j_0=0$) collision. The points are the experimental values of Ref. 12.

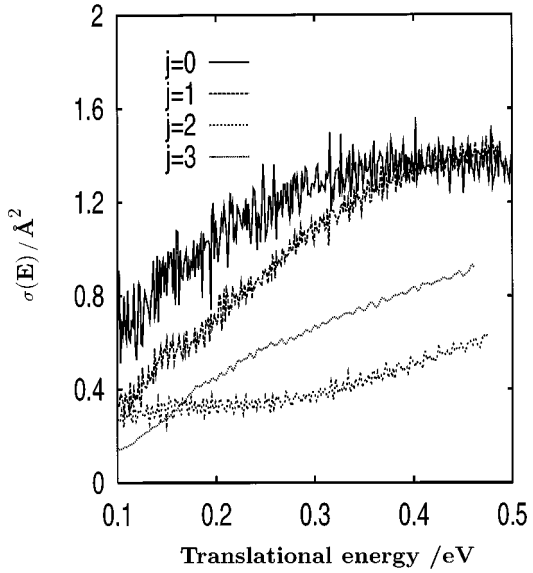

FIG. 12. The total reaction cross section for several initial rotational states of HF($v_0=0$) using the J-shifting approach

proach. The effective shift, however, is roughly half that associated with the transition state, in Eq. (16). This effect is called ''corner cutting'' for reactions of heavy-light-heavy systems.[45] In addition, the mean reaction probability slightly decreases as J increases, thus suggesting that the J-shifting approach will yield higher reaction cross sections.[25]

For $J \geqslant 30$ the background oscillations are softened and the resonant structure nearly disappears. The reason is that the resonances become orbiting, supported by the centrifugal barrier, with very broad widths. The only remaining resonances present an asymmetric structure, a maximum followed by a minimum or vice versa, analogous to the so-called Beutler–Fano profiles appearing in photoionization.[54] By analogy, such a structure is attributed to an interference between two different mechanisms in the dissociation/formation of the quasibound state associated with the orbiting resonance: either by a direct tunneling through the centrifugal barrier or by an indirect transfer of rotational/vibrational energy.

C. Reaction cross sections

In Fig. 11 the reaction cross section for $v_0=0$, $j_0=0$ obtained using the CSA is compared with the available experimental data.[12] The sum over J, in Eq. (15), went up to $J=65$, and is well converged in the whole energy range. The reaction threshold occurs at ≈ 0.06 eV, in agreement with very recent experimental data.[26] Such an effect is only explained when the zero-point energy at the saddle point is included (see Table 1). Particularly interesting is the nonmonotonic behavior of the cross section originated by the oscillations in the background of the reaction probabilities due to quantum interference between the reactant and the product channels. Recent experimental results[26] also show oscillations, which persist even at higher energies, and the first two maxima are approximately placed at the same energies of the CSA results in Fig. 11. Since this oscillatory structure is quite sensitive to the details of the potential interaction we conclude that the PES2 presented in this work is very well adapted to study this reaction.

Recent calculations performed on the PES3, using a similar time-dependent treatment within the CS approach,[23] yielded a reaction cross section slightly lower than that presented in Fig. 11 (see Fig. 6 of Ref. 23). These results[23] also show a reaction threshold and quite a good agreement with the experimental data for the two energies of Ref. 12. However, the results of Ref. 23 do not present oscillations of the cross section as a function of the translational energy.

In crossed-beams experiments the rotational temperature of HF is typically of $\approx$60–80 K. An infrared fluorescence experiment[55] determined that the population of the different rotational states of HF are 0.314, 0.465, 0.189 and 0.032 for $j_0=0$, 1, 2 and 3, respectively. In order to determine the effect of the average on these rotational states, in Fig. 12 we present the reaction cross section for several j_0 values obtained using the J-shifting approach. The J-shifting cross section for j_0 shows some differences with respect to the more accurate CSA results, in Fig. 11. First, the J-shifting approach overestimates the cross section because it does not take into account a slight progressive descent of the reaction probability as a function of J, as it is usually the case.[25] Second, the resonance structure survives in the J shifting, while it nearly disappears in the CSA cross section. Finally, the J shifting erases the background interference oscillations, very evident in the CSA cross section. Despite all these problems, the J-shifting approach provides a reasonable estimate of the magnitude of the cross section and of the role of the rotational average. As it was the case for the reaction probability for $J=0$ discussed above, the results obtained for $j_0=0$ and $j_0=1$ are very close while the cross section for higher j_0's decreases significantly. Since in the incident

beam the major populations are those of $j_0=0$ and 1, and they present very similar cross sections, the average is very close to that of $j_0=0$ and 1. Assuming a similar behavior on the CS approach, we can conclude that the rotationally averaged cross section is similar to that of Fig. 11 but probably lower. In the J-shifting approach it is assumed that the Ω projection only affects by an energy shift on the reaction probability, as it occurs for the case of J. Usually, however, the change on Ω has a stronger effect on the dynamics than the variation of J because it affects more strongly the internal motions.[36] This conclusion needs to be checked by doing the CS and, if possible, exact calculations for higher j_0 and $\Omega_0\neq 0$ to study the effect of the initial projection of j_0 in the z-axis of the body-fixed frame.

V. CONCLUSIONS

In this work a global analytical fit of the potential energy surface of the LiFH system in its ground electronic state is presented, based on a large number (≈2300) of *ab initio* points. This large number of points in the interaction region is necessary to avoid the appearance of artificial details on the fit which strongly affect the reactivity. As an example, it is found that in a previous surface published recently,[22] using about 600 *ab initio* points, there is a repulsive wall in the entance channel, at HF distances larger than expected, which causes a significant reduction of the reactivity. The use of more *ab initio* points to generate the PES2 presented in this work eliminates those artificial barriers and the reaction cross section thus obtained is in agreement with the few experimental values available.[12,26]

The Li+HF reaction is studied using a time-dependent formalism in reactant Jacobi coordinates in a body-fixed frame which allows us to represent the internal coordinates on grids while the Euler angles specifying the orientation of the system are described with a basis set. In this representation the potential become diagonal, thus reducing the memory requirements involved in the calculations. It should be stressed that the procedure is very well suited for massively parallel computing since the only coupling between adjacent helicity channels arises from the Coriolis term.

Using this formalism to calculate the reaction dynamics at $J=5$, the adequacy of the Centrifugal Sudden Approximation was checked in this system. The reaction cross section obtained using the PES2 of this work within the centrifugal sudden approach is in better agreement with the available experimental data[12,26] than for the previous PES's.[19,22] This reaction shows important quantum effects. Its threshold appears at ≈0.06 eV of translational energy which corresponds to the energy of the saddle point plus the zero-point energy, referred to the reactants ground vibrational state. If the zero-point energy was not important, this reaction would not show a threshold since the energy of the saddle point is lower than that of HF in its ground state. In addition, the reaction cross section shows some oscillations originated by the interference between the reactant and product channels, very sensitive to the details of the PES, which also appear in recent experimental data.[26] Moreover, the increase of the reagent rotational excitation produces a decrease on the reaction cross section.

Near the threshold, at low kinetic energies the reaction is dominated by resonances at which the reactivity strongly increases. Since the dipole moment on this system is rather important,[17] the reactivity at those resonances could be directly analyzed after infrared photon excitation (of ≈0.25 eV) from the reactant well. Such kinds of studies will give direct information on the role of intermediate states on the dynamics by determining their lifetimes, structure and possible decay channels. The conditions could therefore be modified, as for example using different excitation pulses, to optimize or change the course of the reaction.

ACKNOWLEDGMENTS

This work has been supported by DGICYT (Ministerio de Educación y Ciencia, Spain) under Grants No. PB94-0160 and No. PB95-0071. We want to acknowledge DGICYT and CIEMAT for the use of a CRAY-J90, and to CCCFC (Universidad Autónoma de Madrid) for the use of a DIGITAL parallel computer. We acknowledge Professor F. J. Aoiz and Professor J. E. Verdasco for very fruitfull discussions and for providing results prior to publication.

[1] E. H. Taylor and S. Datz, J. Chem. Phys. **23**, 1711 (1955).
[2] Z. Karny and R. N. Zare, J. Chem. Phys. **68**, 3360 (1978).
[3] M. Hoffmeister, R. Schleysing, F. Stienkemeier, and H. J. Loesch, J. Chem. Phys. **90**, 3528 (1989).
[4] H. J. Loesch, E. Stenzel, and B. Wüstenbecker, J. Chem. Phys. **95**, 3841 (1991).
[5] H. J. Loesch and F. Stienkemeier, J. Chem. Phys. **99**, 9598 (1993).
[6] Z. Karny, R. C. Estler, and R. N. Zare, J. Chem. Phys. **69**, 5199 (1978).
[7] B. Soep, C. J. Whitham, A. Keller, and J. P. Visticot, Faraday Discuss. Chem. Soc. **91**, 191 (1991).
[8] B. Soep, S. Abbés, A. Keller, and J. P. Visticot, J. Chem. Phys. **96**, 440 (1992).
[9] S. K. Shin, Y. Chen, S. Nckolaisen, S. W. Sharpe, R. A. Beaudet, and C. Wittig, Adv. Photochem. **16**, 249 (1991).
[10] K. Liu, J. C. Polanyi, and S. Yang, J. Chem. Phys. **98**, 5431 (1993).
[11] J. C. Polanyi and J.-X. Wang, J. Chem. Phys. **99**, 13691 (1995).
[12] C. H. Becker, P. Casavecchia, P. W. Tiedemann, J. J. Valentini, and Y. T. Lee, J. Chem. Phys. **73**, 2833 (1980).
[13] H. J. Loesch and F. Stienkemeier, J. Chem. Phys. **98**, 9570 (1993).
[14] W. A. Lester, Jr. and M. Krauss, J. Chem. Phys. **52**, 4775 (1970).
[15] M. M. L. Chen and H. F. Schaefer III, J. Chem. Phys. **72**, 4376 (1980).
[16] C. Suárez, A. Aguado, and M. Paniagua, Chem. Phys. **178**, 357 (1993).
[17] A. Aguado, C. Suárez, and M. Paniagua, Chem. Phys. **201**, 107 (1995).
[18] J. M. Alvariño, M. L. Hernández, E. García, and A. Laganà, J. Chem. Phys. **84**, 3059 (1986).
[19] G. A. Parker, A. Laganà, S. Crocchianti, and R. T Pack, J. Chem. Phys. **102**, 1238 (1995).
[20] M. Baer, I. Last, and H.-J. Loesch, J. Chem. Phys. **101**, 9648 (1994).
[21] F. Gögtas, G. G. Balint-Kurti, and A. R. Offer, J. Chem. Phys. **104**, 7927 (1996).
[22] A. Aguado, M. Paniagua, M. Lara, and O. Roncero, J. Chem. Phys. **106**, 1013 (1997).
[23] W. Zhu, D. Wang, and J. Z. H. Zhang, Theor. Chem. Acc. **96**, 31, (1997).
[24] A. Aguado and M. Paniagua, J. Chem. Phys. **96**, 1265 (1992).
[25] J. M. Bowman, Adv. Chem. Phys. **61**, 115 (1985).
[26] F. J. Aoiz, M. Menéndez, J. E. Verdasco, Sáez-Rabanos, H. J. Loesch, F. Stienkemieir, B. Berning, and H. J. Werner, submitted to J. Phys. Chem.
[27] R. N. Zare, *Angular Momentum* (Wiley, New York, 1988).
[28] G. C. Schatz and A. Kuppermann, J. Chem. Phys. **65**, 4642 (1976).
[29] H. Tal-Ezer and R. Kosloff, J. Chem. Phys. **81**, 3967 (1984).
[30] R. Kosloff, J. Chem. Phys. **92**, 2087 (1988).

[31] J. C. Light, I. P. Hamilton, and J. V. Lill, J. Chem. Phys. **82**, 1400 (1985).
[32] A. C. Peet and W. Yang, J. Chem. Phys. **91**, 6598 (1989).
[33] J. T. Muckerman, Chem. Phys. Lett. **173**, 200 (1990).
[34] G. C. Corey, J. W. Tromp, and D. Lemoine, '' Fast pseudospectral algorithm in curvilinear coordinates,'' in *Numerical Grid Methods and their Application to Schrödinger Equation*, edited by C. Cerjan (Kluwer Academic, New York, 1993), p. 1.
[35] O. A. Sharafeddin and J. C. Light, J. Chem. Phys. **102**, 3622 (1995).
[36] O. Roncero, D. Caloto, K. C. Janda, and N. Halberstadt, J. Chem. Phys. **107**, 1406 (1997).
[37] W. H. Miller, J. Chem. Phys. **61**, 1823 (1974).
[38] D. H. Zhang and J. Z. H. Zhang, J. Chem. Phys. **101**, 3672 (1994).
[39] D. Neuhauser, J. Chem. Phys. **100**, 9272 (1994).
[40] E. M. Goldfield, S. K. Gray, and G. C. Schatz, J. Chem. Phys. **102**, 8807 (1995).
[41] J. Z. H. Zhang and W. H. Miller, J. Chem. Phys. **91**, 1528 (1989).
[42] R. T. Pack, J. Chem. Phys. **60**, 633 (1974).
[43] P. McGuire and D. J. Kouri, J. Chem. Phys. **60**, 2488 (1974).
[44] G. C. Schatz, D. Sokolovski, and J. N. L. Connor, J. Chem. Phys. **94**, 4011 (1990).
[45] Q. Sun, J. M. Bowman, G. C. Schatz, J. R. Sharp, and J. N. L. Connor, J. Chem. Phys. **92**, 1677 (1990).
[46] R. J. Buenker, '' Studies in physical and theoretical chemistry.'' in *Current Aspects of Quantum Chemistry*, edited by R. Carbó (Elsevier, Amsterdam, 1982), Vol. 21.
[47] Electronic mail: Miguel.Paniagua@uam.es.
[48] G. G. Balint-Kurti, R. N. Dixon, and C. C. Marston, J. Chem. Soc. Faraday Trans. **86**, 1741 (1990).
[49] G. G. Balint-Kurti, F. Gögtas, S. P. Mort, A. R. Offer, A. Laganà, and O. Gervasi, J. Chem. Phys. **99**, 9567 (1993).
[50] N. Sathyamurty, Chem. Rev. **83**, 601 (1983).
[51] H. J. Loesch, Chem. Phys. **104**, 213 (1986).
[52] J. A. Harrison and H. R. Mayne, Chem. Phys. Lett. **158**, 356 (1989).
[53] F. J. Aoiz and J. E. Verdasco (personal communication).
[54] U. Fano, Phys. Rev. **124**, 1866 (1961).
[55] M. Brinkhoff, Diplomarbeit, Universität Bielefeld, 1986.